applied sciences

MDPI

Article

Understanding Electromagnetic Interactions and Electron Transfer in Ga Nanoparticle–Graphene–Metal Substrate Sandwich Systems

Yael Gutiérrez [1,2,*], Maria M. Giangregorio [1], April S. Brown [3], Fernando Moreno [1,2] and Maria Losurdo [1,*]

1 Institute of Nanotechnology, CNR-NANOTEC, Via Orabona 4, 70126 Bari, Italy; michelaria.giangregorio@nanotec.cnr.it (M.M.G.); morenof@unican.es (F.M.)
2 Department of Applied Physics, University of Cantabria, Avda. Los Castros, s/n., 39005 Santander, Spain
3 Electrical and Computer Engineering Department, Duke University, Durham, NC 27728, USA; april.brown@duke.edu
* Correspondence: gvelay@unican.es (Y.G.); maria.losurdo@cnr.it (M.L.)

Received: 27 August 2019; Accepted: 29 September 2019; Published: 30 September 2019

Abstract: Plasmonic metal nanoparticle (NP)–graphene (G) systems are of great interest due their potential role in applications as surface-enhanced spectroscopies, enhanced photodetection, and photocatalysis. Most of these studies have been performed using noble metal NPs of silver and gold. However, recent studies have demonstrated that the noble metal–graphene interaction leads to strong distortions of the graphene sheet. In order to overcome this issue, we propose the use of Ga NPs that, due to their weak interaction with graphene, do not produce any deformation of the graphene layers. Here, we analyze systems consisting of Ga NP/G/metal sandwich coupling structures, with the metal substrate being, specifically, copper (Cu) and nickel (Ni), i.e., Ga NP/G/Cu and Ga NPs/G/Ni. We experimentally show through real-time plasmonic spectroscopic ellipsometry and Raman spectroscopy measurements of the quenching of the Ga NP localized surface plasmon resonance (LSPR) depending on the wetting of the graphene by the Ga NPs and on the electron transfer through graphene. Theoretical finite-difference time-domain (FDTD) simulations supportively demonstrate that the LSPR in such sandwich structures strongly depends on the contact angle of the NP with graphene. Finally, we also provide evidence of the electron transfer from the Ga NPs into the graphene and into the metal substrate according to the work function alignments. These considerations about the contact angle and, consequently, geometry and wetting of the metal NPs on graphene, are useful to guide the design of those plasmonic systems to maximize electromagnetic enhancement.

Keywords: graphene; gallium nanoparticles; plasmonics; copper; nickel

1. Introduction

Several plasmonic metal nanoparticle–graphene systems have been reported in the literature for applications in surface-enhanced Raman spectroscopy (SERS) [1,2], photodetection [3], enhanced biosensing, and photocatalysis, among others. Indeed, in analyzing this literature, the use of pristine graphene (G) or graphene oxide (GO) should also be noted [4,5], the latter always presenting some defects and some oxygen functional groups such as COOH, COH, and COH at the reduced graphene oxide surface. Different oxidizing agents lead to various carbon-to-oxygen ratios and chemical compositions in GO and, consequently, to a different surface energy of graphene and GO, which contributes to the hydrophobic character of graphene and to the hydrophilic character of GO, thereby

differently affecting the anchoring and coupling to plasmonic metal nanoparticles (NPs). Furthermore, most of these systems rely on noble plasmonic metals such as gold (Au) and silver (Ag), and again, in comparing literature in the field of graphene-plasmonic Au NPs, attention should be paid to whether Au NPs are pure or stabilized/decorated by surfactant and functionalizing agents, which also affects the graphene/NP interface and coupling [6]. Indeed, the use of Au and Ag metals on pristine graphene entails some problems. For instance, when Au film is in physical contact with graphene, delamination can easily occur at the contact interface. Furthermore, *d*-valence electrons of noble metals exhibit covalent bonding on the top (T) site of the graphene structure with strong hybridization of the adatom and graphene electronic states, which leads to a strong distortion and changes the graphene sp^2-like C to a more covalent reactive sp^3-like C [3,7]. This strong interaction has also been reported to significantly modify the band structure and Dirac cones of graphene [8]. For example, in Ag NP/G/Ag systems the appearance of the D band in the Raman spectra of graphene has been reported due to the defects caused by the graphene–Ag interaction [2]. On the contrary, research on finding non-noble plasmonic metals is expanding [9], and among these, elements from groups XIII (i.e., Ga) are interesting since calculations predict [7] that Ga adsorbs on the hollow (H) site of graphene and does not distort the graphene sheet, so the C–C bonds near the adatom retain their sp^2 character. Therefore, the use of this type of plasmonic metals presents advantages with respect to the widely used noble metals. Moreover, the plasmonic properties of Ga have been demonstrated to be superior to those of Ag, Au, or Cu due to its chemical stability (Ga forms a 1 nm oxide shell thickness that protects and keeps the NPs stable for years [10]) and the spectral tunability of the plasmon peak from the near-IR to the UV [11] (Ag, Au, and Cu have an interband transition in UV that inhibit a plasmonic response in this spectral region [12]).

Furthermore, among the various configurations, the metal/graphene/metal sandwich coupling system has gained interest for using the graphene layer as a controlled nano-spacer [1,2,13,14]. The reason for this is the strong local field enhancement achieved by the multiple couplings produced, including the NP–NP coupling and NP–metal film coupling through the graphene that further strengthens the electromagnetic field [1,2]. Examples of this sandwich plasmonic graphene system are the all-Ag Ag NP/G/Ag [2] and all-Cu Cu NP/G/Cu [1] sandwich systems, which can be considered almost symmetric configurations in the sense that the metals on the two sides of graphene have the same work function.

In this work, we analyze the Ga NP/graphene/Cu and the Ga NP/graphene/Ni sandwich structures. These systems present several advantages: (*i*) Ga NPs do not damage the graphene structure [15]; (*ii*) the used pristine graphene is directly chemical vapor deposition (CVD)-grown on Cu and Ni substrates, consequently avoiding its transfer, a process that can introduce defects and impurities into the graphene [16] and lead to imperfect contact between graphene and the metal layer underneath, generating an additional barrier, and increases the contact resistance for electrons when passing through the graphene/metal layer contact interface; (*iii*) the Ga NPs are evaporated directly on graphene under vacuum, without the use of any surfactant or capping/functionalizing agents, allowing the investigation of the bare graphene/NP interface. Therefore, the idea consists of investigating the plasmonic coupling of Ga NPs on pristine CVD-grown graphene/Cu and graphene/Ni, those two systems also being characterized by an asymmetry in work function of the two metals in contact with graphene and by different layers of the grown graphene spacer, monolayer in the former case and multilayer in the latter case.

The additional peculiarity of this study is the in-situ real-time probing of the Ga NP/G interaction during the growth of the Ga NPs on the graphene surface. Specifically, the interaction of the Ga NP/G/Cu and Ga NP/G/Ni systems with light and the generation of surface plasmon resonances are studied in real time by spectroscopic ellipsometry and compared with Ga NP/G/glass [15]. We demonstrate that there is no appearance of surface plasmon resonances in the work-function asymmetric graphene–metal sandwich systems, and we theoretically show that this process strongly depends on the contact angle between the metal NPs and the G/metal substrate, a parameter determined by the interfacial free energy between the nanoparticle and the graphene layer. The quenching of the localized surface

plasmon resonance (LSPR) of the Ga NPs is also corroborated by evidence based on Raman and X-Ray photoelectron spectroscopies of the electron transfer from the Ga NPs into the graphene and, finally, into the metallic substrate.

2. Materials and Methods

2.1. Sample Preparation

Graphene (G) was grown by chemical vapor deposition (CVD) from mixtures of CH_4:H_2 = 100:0–50 sccm gases at a temperature of 900 °C and at a total pressure of 4 Torr. The samples were then cooled at a rate of ≈2 °C min^{-1} in 1 Torr of H_2 [16].

Copper (Cu) foils of 30 μm thickness from Alfa Aesar (Ward Hill, MA, U.S.) and 300 nm Ni/300 nm SiO_2/Si obtained by sputtering were used as substrates. They were pre-annealed at 400 °C in ultra-high vacuum (UHV) for nickel and copper oxide desorption and then heated to 900 °C in 1 Torr of H_2 for recrystallization. As verified by Raman spectroscopy analysis, the graphene grown on Cu was a monolayer (1L), while the graphene on Ni was a non-homogeneous distribution of monolayer, bilayer, and multilayer graphene [11].

After graphene growth, the samples were transferred under vacuum in a Veeco GEN II molecular beam epitaxial system where Ga nanoparticles (Ga NPs) were deposited onto the graphene under UHV conditions. The nanoparticles were deposited at room temperature with a constant Ga flux equivalent to 82 monolayers (MLs) per minute as determined using a thin film approximation. This process assured very clean interfaces between the Ga NPs and the graphene, as well as between the graphene and the underlying metallic layer.

For comparison, Ga NPs were also simultaneously deposited on 1 ML graphene grown on Cu and transferred by the tape method [15] on a glass substrate to be used as a control sample for the plasmon resonance of the Ga NPs.

2.2. Sample Characterization

Raman spectroscopy has proven to be a powerful tool to evaluate the quality and thickness of graphene layers [17]. Raman spectra were collected using a LabRAM HR Horiba-Jobin Yvon spectrometer with 532 nm excitation under ambient conditions at low laser power (<1 mW).

The chemical species analysis was carried out using X-ray photoelectron spectroscopy (XPS) using a monochromatic Al Kα source (PHI 5400 VERSAPROBE) at a take-off angle of 45°. The main core photoelectron levels investigated were the C1s and the Ga3d, to evaluate the metallicity of the Ga NPs and any electron transfer between the Ga NPs and the graphene layer.

The Ga NPs were imaged using atomic force microscopy (AFM) performed using an AutoProbe CP ThermoMicroscope.

Ellipsometric spectra of the complex pseudo dielectric function, $\langle\epsilon\rangle = \langle\epsilon_1\rangle + i\langle\epsilon_2\rangle$, and of the extinction coefficient $\langle k\rangle$, being $\langle\epsilon\rangle = \langle\epsilon_1\rangle + i\langle\epsilon_2\rangle = (\langle n\rangle + i\langle k\rangle)^2$, where n is the real part of the refractive index, were acquired using a phase-modulated spectroscopic ellipsometer (UVISEL, Horiba-Jobin Yvon) in the 0.75–6.0 eV spectral range with a resolution of 0.01 eV to monitor the plasmon resonance behavior of the Ga NPs on G/Cu and Ga NPs on G/Ni structures. Ellipsometric spectra were also acquired in real time during the Ga NP deposition, with each spectrum acquired every 1 s.

2.3. Electromagnetic Simulations

Maxwell's equations were solved using finite-difference time-domain (FDTD) methods as implemented in the commercial software FDTD solutions Version 8.16 from Lumerical Inc. The dielectric function of Ga, Cu, and Ni was taken from different sources in the literature [10,18]. The graphene monolayer was modeled using a surface conductivity approach. The surface conductivity for a single layer of graphene is given by the expression provided by Hanson in [19].

Total field/scattered field light source conditions were used in all simulations. An illuminating linearly polarized plane-wave was set to propagate perpendicular to the substrate. The wavelength spectral range analyzed was from 200 to 1000 nm to mimic experimental conditions. A non-uniform mesh was used in the simulation region. A finer mesh was defined in the vicinity of the NPs. In this region, the mesh step was fixed to $d_x = d_y = d_z = 1$ nm. The absorption cross-section was calculated within the total-field/scattered-field formalism.

3. Results

3.1. Ga Nanoparticles on Graphene/Glass

First, as a reference system, we consider the case of Ga NPs deposited on a monolayer (ML) of graphene on an insulating glass substrate. Figure 1a shows the real-time evolution of the pseudo extinction coefficient $\langle k \rangle$ during the Ga NP deposition on the G/glass substrate. As the Ga deposition over the substrate increases (white arrow in the figure), a peak associated with an LSPR appears in the $\langle k \rangle$ spectra. The LSPR peak red-shifts and increases in amplitude with deposition time, consistently with the increase in the size of the Ga NPs [10,11], whose final morphology is shown as an inset in the same figure. The Ga NPs have a hemispherical shape, and their diameter has been estimated to be 50–60 nm through AFM. The excited LSPR corresponds to the so-called longitudinal (LO) mode, while the transverse mode (TO) is at energies higher than 7 eV and, therefore, is out of the measurement range [10,11]. Figure 1b shows the typical near-field distribution of a hemispherical Ga NP on a G/glass substrate excited at the LO mode. The near-field map shows a strong localization of the electromagnetic field (hotspots) at the interface between the Ga NPs and the G/glass substrate. In fact, these hotspots have been proven to enhance the Raman signal of the graphene layer. Figure 1c shows the graphene Raman spectra before and after Ga NP deposition. Interestingly, the spectra are dominated by the characteristic G and 2D bands of graphene, respectively at 1583 cm^{-1} and 2698 cm^{-1}, with a characteristic intensity ratio typical of 1 monolayer (1ML) graphene and without any significant peak D (at ~1350 cm^{-1}) indicative of defects, demonstrating that the good quality of the graphene CVD-grown on Cu foil is preserved after being transferred to the glass substrate and the Ga NP deposition. It can also be seen how the intensity of the Raman peaks of graphene on glass is significantly enhanced by the Ga NPs due to the electromagnetic enhancement and hot spots localized at the Ga NP/G interface, as shown in Figure 1b. For both the G and 2D peaks, the intensity increases more than one order of magnitude.

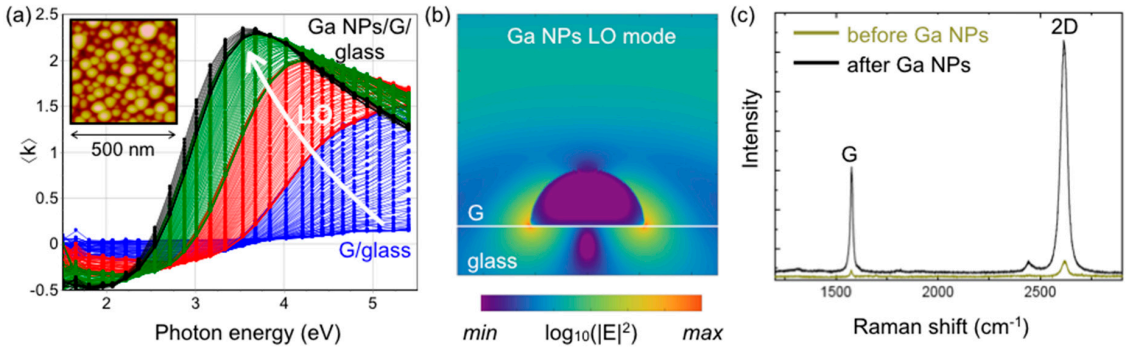

Figure 1. Ga nanoparticles (NPs) on G/glass substrate. (**a**) Extinction coefficient spectra $\langle k \rangle$ recorded in real time during Ga NP deposition on the G/glass substrate; the first blue spectrum refers to G/glass, while the last black spectrum refers to the Ga NPs/G/glass; the arrow indicates Ga NP deposition. As an inset is shown an atomic force microscopy (AFM) image of the Ga NP morphology. (**b**) Near-field distribution of the electromagnetic field when the Ga NPs are excited at their longitudinal (LO) mode. (**c**) Raman spectra of the graphene layer/glass before and after Ga NP deposition.

3.2. Ga Nanoparticles on Graphene/Cu

In contrast to the glass insulating substrate, here we study the effect of having a conducting substrate such as Cu. Specifically, the system analyzed consists of Ga NPs on monolayer graphene/Cu. In this system, the Ga NPs are deposited directly on the CVD-grown graphene/Cu. In this way, we avoid the graphene transfer that could contaminate or damage it. Figure 2a shows the real-time evolution of the pseudo-extinction coefficient $\langle k \rangle$ during Ga NP deposition on the G/Cu support. For comparison, the spectrum $\langle k \rangle$ of equivalent Ga NPs simultaneously deposited on G/glass is also plotted, showing that the same NPs should give an LSPR peak at approximately 3.3 eV. The first spectrum (blue in Figure 2a) represents the G/Cu system, and its overall shape is significantly different from that of G/glass in Figure 1a because of the dielectric function of copper, i.e., the spectral region below 2 eV is representative of the Drude component of Cu free carriers, while above 2eV, the spectra show the Cu interband transitions [13] smoothed and decreased by the absorption of graphene. Although Ga NPs are formed on the G/Cu, as shown by the SEM tilted picture shown in Figure 2a, it is clear that when the Ga NPs are on the G/Cu support, there is no excitation of the LO mode. Figure 2b shows the calculated absorption cross-section spectra of Ga NPs on G/glass and G/Cu substrates. It can be seen that when going from the G/glass to the G/Cu substrate, the LSPR is completely quenched. This is consistent with the fact that both G and Cu are conducting, and thus no confinement is produced at the Ga NP-graphene/Cu interface. These results are corroborated by electromagnetic simulations on a Ga hemisphere on the G/Cu substrate illuminated under normal incidence. As shown in Figure 2c, the near-field maps are completely different for the two cases.

Specifically, while Ga NPs on G/glass show a high near-field enhancement at the interface between NP and substrate, for the G/Cu the near-field distribution is uniform around the particle, being minimal at the top of NPs. Therefore, in this case, hotspots at the NP–substrate interface that can enhance the Raman signal of the graphene layer are not produced. Consistently, as shown in Figure 2d, there is no enhancement of the Raman signal of the graphene layer before and after deposition of the Ga NPs on the G/Cu substrate. A deeper analysis of the position of the 2D peak measured for different deposited Ga amounts, as reported in Figure 2e, shows a shift of the 2D peak to a lower wavenumber with the increase of Ga. This phenomenon can be explained considering electron transfer from the Ga NPs into the graphene layer and, consequently, an n-type doping of the graphene layer [20]. This electron transfer is also supported by the XPS analysis. Figure 2f shows the spectra of the photoelectron core level Ga3*d* on G/Cu (red curve) compared to that of Ga NPs on an insulating glass substrate (blue curve). It can be seen that in both cases, the Ga3*d* photoelectron level shows two main components, namely, the component at binding energy BE = 18 eV due to metallic gallium, Ga^0, and the one at a the higher binding energy BE= 20.8 eV due to oxidized gallium, Ga^{3+} [21]. For Ga NPs on insulating glass, the Ga is mainly in the metallic state, which is consistent with the evidence of the localized plasmon resonance peak; conversely, for Ga NPs on G/Cu, the Ga^{3+} is the main component, which is consistent with the loss of electrons in the Ga NPs deriving into cationic character. This electron transfer from Ga NPs to graphene and then into the Cu substrate, due to the conductivity of substrates, is consistent with the values of the work function ϕ_F of each of the involved materials (ϕ_F^{Ga} = 4.2 eV, ϕ_F^{G} = 4.5 eV and ϕ_F^{Cu} = 4.9 eV), as depicted in the schema in Figure 3a. Therefore, the transferred electrons are moved into lower energy states.

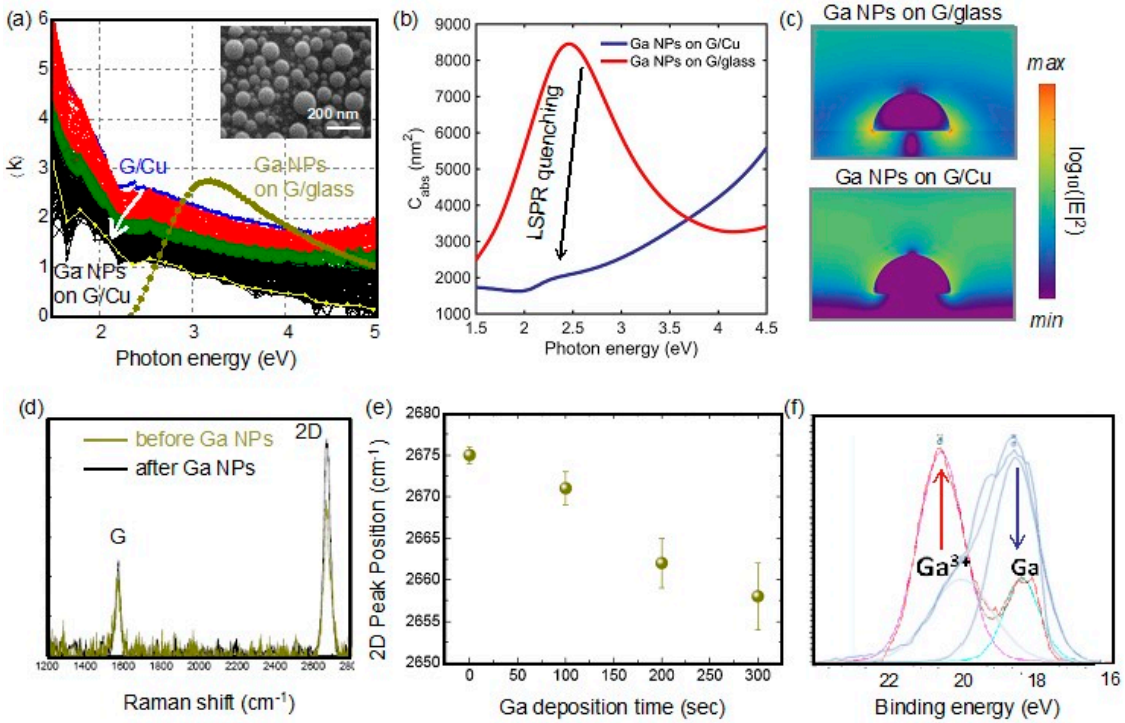

Figure 2. Ga NPs on G/Cu support. (**a**) Experimental extinction coefficient spectra $\langle k \rangle$ recorded in real time during Ga NP deposition on the G/Cu substrate. Each spectrum is acquired every 1 sec; the blue spectrum refers to the initial G/Cu sample, while the last yellow spectrum refers to the Ga NP/G/Cu; the arrow indicates Ga NP deposition. For comparison, the $\langle k \rangle$ spectra for Ga NPs on G/glass are also shown. As an inset is shown an SEM image of the NP morphology. (**b**) Calculated absorption cross-section of a R = 55 nm Ga hemisphere on G/Cu and G/glass substrates illuminated under normal incidence. (**c**) Near-field distribution of the electromagnetic field when the Ga NPs are excited at 3 eV when deposited on G/Cu (bottom) and G/glass substrates (top). (**d**) Raman spectra of the graphene layer before and after Ga NP deposition. (**e**) Graphene 2D band position as a function of Ga deposition time. (**f**) X-ray photoelectron spectroscopy (XPS) spectra of the photoelectron core level Ga3*d* on G/Cu (red curve) compared to that of Ga NPs on an insulating glass substrate (blue curve).

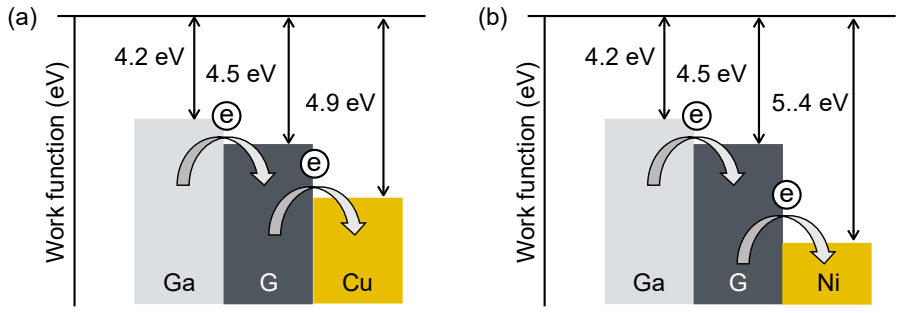

Figure 3. Schema of the work function ϕ_F and of electron transfer in the systems (**a**) Ga NP/G/Cu and (**b**) Ga NP/G/Ni

3.3. Ga Nanoparticles on Graphene/Ni

In order to demonstrate that the Ga NP/G/Cu is not a particular case and to investigate the role of the thickness of graphene, we also investigated Ga NPs on G/Ni, since it is known that the main difference between the CVD growth of graphene on Cu and Ni is that graphene is limited to a monolayer on Cu, while multilayer graphene grows on Ni. Results very similar to those of the

Ga NP/G/Cu system were obtained for Ga NP/G/Ni, although in the latter, the graphene layer is a non-homogeneous mixture of bilayer and multilayer regions. Figure 4a shows the real-time evolution of the pseudo-extinction coefficient $\langle k \rangle$ during Ga NP deposition on G/Ni. For comparison, the $\langle k \rangle$ spectrum of equivalent Ga NPs grown simultaneously on G/glass is also shown. As in the case of G/Cu, there is no plasmon resonance peak coming from the excitation of the LSPR LO mode of the Ga NPs, although Ga NPs are clearly formed on the substrate, as demonstrated by the AFM image in the inset of Figure 4c. This behavior is consistent with the fact that G/Ni is also a conductor, like G/Cu. The experimental spectra show a damping of the Ni's characteristic Drude-like behavior at low photon energies as well as of the peak above 4 eV coming from the interband transition of Ni [18] due to the effective thickness of the Ga NPs. The absence of any localized surface plasmon resonance in the extinction coefficient spectra is consistent with the absence of any enhancement of the Raman signal of the graphene layer, as shown in Figure 4b. Here, the variation of the intensity ratio between the G and 2D peak is not speculated because it might be due to the non-homogeneity of the graphene layer thickness. Moreover, the XPS analysis of the photoelectron core lever Ga3*d* also shows, in this case, a strong Ga^{3+} (BE = 20.8 eV) component and a quenched metallic Ga component (BE = 18 eV) [21]. This puts in evidence the loss of the metallic character of the Ga NPs due to electron transfer from the Ga NPs into the graphene and finally into the Ni substrate, according to the schema sketched in Figure 3. As shown in Figure 3b, Ga, G, and Ni have values of their work functions of $\phi_F^{Ga} = 4.2$ eV, $\phi_F^{G} = 4.5$ eV, and $\phi_F^{Cu} = 5.4$ eV, respectively; thus, electrons transfer from the Ga NPs to graphene and to nickel.

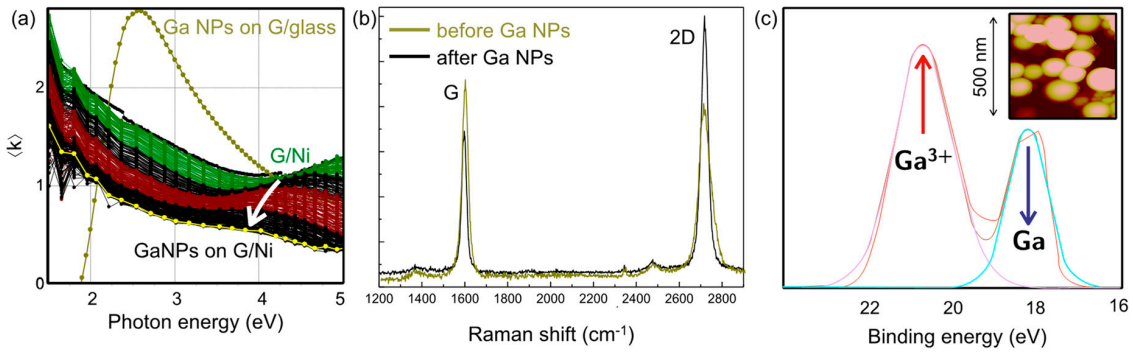

Figure 4. Ga NPs on G/Ni support. (**a**) Experimental extinction coefficient spectra $\langle k \rangle$ recorded in real time during Ga NP deposition on the G/Ni substrate. Each spectrum is acquired every 1 sec; the black spectrum refers to the initial G/Ni sample; the final yellow spectrum refers to Ga NP/G/Ni; the arrow indicates Ga NP deposition. For comparison, the $\langle k \rangle$ spectra for equivalent Ga NPs on G/glass is also shown. (**b**) Raman spectra of the graphene layer before and after Ga NP deposition. (**c**) XPS spectra of the photoelectron core level Ga3*d* for Ga/G/Ni. The inset shows the AFM image of the Ga NP morphology.

4. Effect of Nanoparticle Shape: Contact Angle between Ga NPs and Graphene

A critical issue when considering the near-field enhancement produced in metal nanoparticle–graphene–metal substrate systems is the contact angle, θ_c, between the NP and the graphene (see Figure 5a). When metal NPs are evaporated on graphene, as in Refs. [1–3], their contact angle with the graphene layer is related to their interfacial free energy. Common plasmonic noble metals such as Au, Ag, and Cu present values of the contact angle with graphene of 113° [22], 114° [23], and 122° [24], respectively. It is also worth mentioning that while for Ag the contact angle remains stable in time [23], for copper the contact angle progressively reduces to a value of 60° in 30 min [24]. In the case of Ga, the contact angle with smooth graphene layers, like the ones in our experiments, is close to a hemispherical NP shape, ~80°. However, for rough and rippled graphene surfaces, the value of the contact angle can go up to 150°. The contact angle that defines the shape of the NP is a key parameter to be considered when modeling the electromagnetic interactions in this type of system [25].

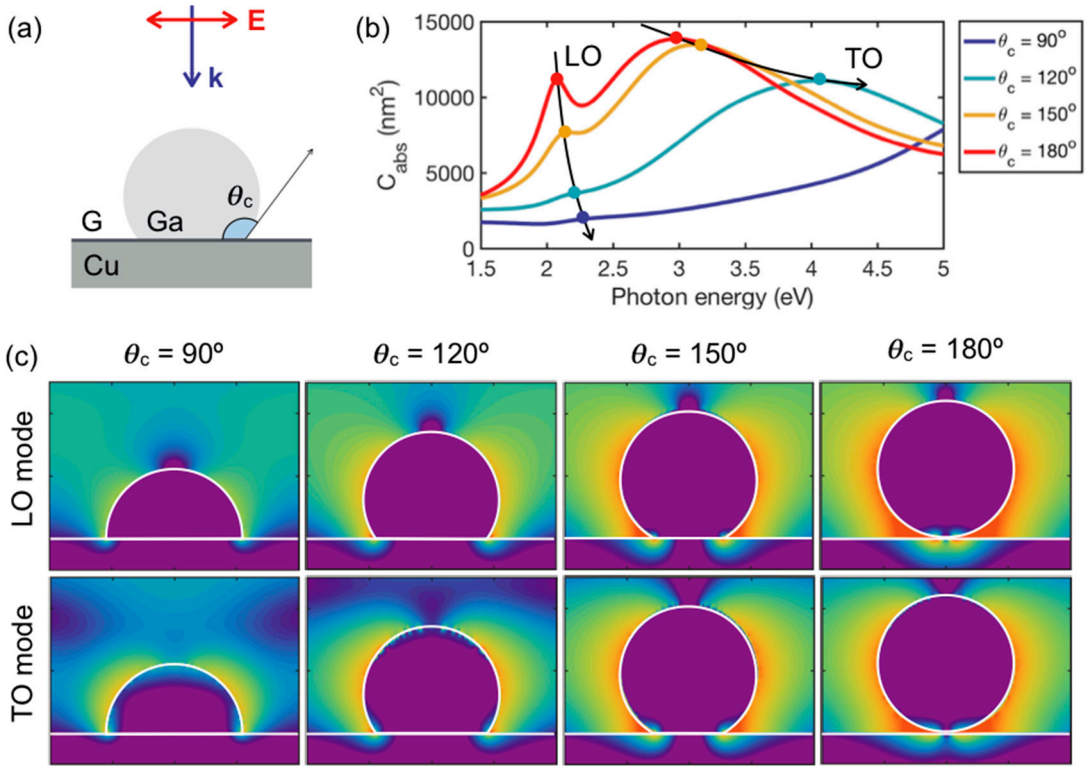

Figure 5. Electromagnetic simulations for the Ga NP/G/Cu system at different values of contact angle, θ_c, between Ga NPs and the G/Cu substrate. (**a**) Schema of the simulated geometry: Ga NP on G/Cu forming a contact angle θ_c illuminated under normal incidence (**k**, blue arrow) with linearly polarized light (**E**, red arrow). (**b**) Absorption cross-section, C_{abs}, of Ga NPs on G/Cu with different contact angles θ_c. (**c**) Near-field maps, $log_{10}(|E|^2)$, at the longitudinal (LO) and transverse mode (TO) modes of Ga NPs on G/Cu with different contact angles θ_c.

In light of this, Figure 5b shows the absorption cross-section C_{abs} of spherical Ga NPs of R = 55 nm illuminated at normal incidence (see sketch in Figure 5a) forming different contact angles with a G/Cu substrate: 90° (hemisphere), 120°, 150° and 180° (sphere). The C_{abs} spectra for the sphere (θ_c = 180°) show two clear resonant peaks: a low-energy peak associated with a dipolar mode (related to the LO mode in the hemisphere), and a high-energy one associated with a higher-order mode (related to the TO mode in the hemisphere). The dipolar mode (LO) progressively quenches and slightly blue-shifts with the decrease of θ_c, while the higher-order plasmon mode (TO) is severely blue-shifted and damped. The near-field distribution in Figure 5c shows high enhancement at the NP–substrate boundary for the spherical nanoparticle, which decreases with the decrease in θ_c (going from the spherical to the hemispherical geometry). One of the factors affecting the near-field enhancement is the contrast between the optical properties of the NP and its surrounding medium (electromagnetic boundary conditions). Dipolar modes are produced by oscillations of the electrons at the equatorial plane of the spherical NP. For high values of θ_c, the effective surrounding medium around the equatorial plane of the NP is air (high contrast, metal–insulator) leading to high near-field enhancements. This effect is additionally enhanced by the coupling of the mode to the cavity formed in the NP–air–substrate region. Moving to the hemispherical shape (decreasing values of θ_c), the contrast between the NP and the surrounding medium decreases due to the proximity of the conducting substrate, and the near-field enhancement becomes lower. Moreover, the cavity region becomes smaller, hampering the coupling of the mode until its full disappearance at θ_c = 90°. It is worth mentioning that this mode is relevant for SERS applications [1,2]. The high-energy mode (TO mode) also shows a near-field enhancement distribution concentrated at the NP–substrate interface for the spherical case (θ_c = 180°), due to its

coupling with the cavity. As θ_c decreases, the mode gets concentrated at the nanoparticle surface, which is consistent with its TO-mode character [26].

5. Conclusions

Ga NPs were deposited on CVD graphene grown on Cu and Ni substrates. These Ga NP/ G/Cu and Ga NP/G/Ni systems present two advantages: (*i*) Ga NPs do not distort the graphene layer, and (*ii*) the graphene layers are directly CVD-grown on the Cu and Ni, consequently avoiding a transfer step that may introduce defects and impurities in graphene. Using spectroscopy ellipsometry and Raman spectroscopy, we demonstrated that neither an LSPR peak is present in the ellipsometric spectra nor is enhancement of the graphene Raman signal produced. It was shown that a critical factor to achieve LSPR and electromagnetic enhancement in these metal NP/G/metal layer sandwich systems is the contact angle between the NPs and the G/metal, which in turn is determined by the interfacial free energy between the two media. NPs need to have a high contact angle with graphene to produce high near-field enhancements at the NP–substrate interface. Finally, through Raman and X-ray photoelectron spectroscopies, we demonstrated that for hemispherical NPs, when the contact area between the NP and the graphene is highest, electron transfer from the Ga NPs to graphene and to the Cu or Ni substrate also contributes to the LSPR quenching. This phenomenon is clearly evidenced by the Ga3*d* photoelectron core level of the nanoparticles, showing a decrease in the metallic Ga^0 component and an increase in the Ga^{3+} component. These considerations may be used to guide the design of plasmonic NP/graphene/metal layer systems to achieve maximum electromagnetic enhancement, by increasing the contact angle between the NPs and the graphene/metal support.

Author Contributions: Y.G. and M.L. wrote the paper. Y.G. and F.M. designed the electromagnetic simulations. Y.G. performed the electromagnetic simulations. A.S.B. and M.L. conceived and designed the experiments. M.M.G. and M.L. performed the growth of samples experiments and the characterizations of the samples.

Funding: This research received no external funding.

Acknowledgments: All authors are grateful to Dr. Giovanni Bruno and Mr. Alberto Sacchetti for their assistance in the CVD growth of graphene. Y.G. thanks the University of Cantabria for her FPU grant.

Conflicts of Interest: The authors declare no conflict of interest.

References

1. Li, X.; Ren, X.; Zhang, Y.; Choy, W.C.H.; Wei, B. An all-copper plasmonic sandwich system obtained through directly depositing copper NPs on a CVD grown graphene/copper film and its application in SERS. *Nanoscale* **2015**, *7*, 11291–11299. [CrossRef] [PubMed]
2. Li, X.; Choy, W.C.H.; Ren, X.; Zhang, D.; Lu, H. Highly intensified surface enhanced raman scattering by using monolayer graphene as the nanospacer of metal film-metal nanoparticle coupling system. *Adv. Funct. Mater.* **2014**, *24*, 3114–3122. [CrossRef]
3. Liu, Y.; Cheng, R.; Liao, L.; Zhou, H.; Bai, J.; Liu, G.; Liu, L.; Huang, Y.; Duan, X. Plasmon resonance enhanced multicolour photodetection by graphene. *Nat. Commun.* **2011**, *2*, 577–579. [CrossRef] [PubMed]
4. Wang, Y.; Polavarapu, L.; Liz-Marzán, L.M. Reduced Graphene Oxide-Supported Gold Nanostars for Improved SERS Sensing and Drug Delivery. *ACS Appl. Mater. Interfaces* **2014**, *6*, 21798–21805. [CrossRef]
5. Lee, Y.H.; Polavarapu, L.; Gao, N.; Yuan, P.; Xu, Q.H. Enhanced optical properties of graphene oxide-Au nanocrystal composites. *Langmuir* **2012**, *28*, 321–326. [CrossRef] [PubMed]
6. Khalil, I.; Julkapli, N.M.; Yehye, W.A.; Basirun, W.J.; Bhargava, S.K. Graphene-gold nanoparticles hybrid-synthesis, functionalization, and application in a electrochemical and surface-enhanced raman scattering biosensor. *Materials* **2016**, *9*, 406. [CrossRef]
7. Chan, K.T.; Neaton, J.B.; Cohen, M.L. First-principles study of metal adatom adsorption on graphene. *Phys. Rev. B Condens. Matter Mater. Phys.* **2008**, *77*, 1–12. [CrossRef]
8. Subrahmanyam, K.S.; Manna, A.K.; Pati, S.K.; Rao, C.N.R. A study of graphene decorated with metal nanoparticles. *Chem. Phys. Lett.* **2010**, *497*, 70–75. [CrossRef]

9. Blaber, M.G.; Arnold, M.D.; Ford, M.J. A review of the optical properties of alloys and intermetallics for plasmonics. *J. Phys. Condens. Matter* **2010**, *22*, 143201. [CrossRef]
10. Losurdo, M.; Suvorova, A.; Rubanov, S.; Hingerl, K.; Brown, A.S. Thermally stable coexistence of liquid and solid phases in gallium nanoparticles. *Nat. Mater.* **2016**, *15*, 995–1002. [CrossRef]
11. Wu, P.C.; Kim, T.-H.; Brown, A.S.; Losurdo, M.; Bruno, G.; Everitt, H.O. Real-time plasmon resonance tuning of liquid Ga nanoparticles by in situ spectroscopic ellipsometry. *Appl. Phys. Lett.* **2007**, *90*, 103119. [CrossRef]
12. Sanz, J.M.; Ortiz, D.; Alcaraz de la Osa, R.; Saiz, J.M.; González, F.; Brown, A.; Losurdo, M.; Everitt, H.O.; Moreno, F. UV Plasmonic Behavior of Various Metal Nanoparticles in the Near- and Far-Field Regimes: Geometry and Substrate Effects. *J. Phys. Chem. C* **2013**, *117*, 19606–19615. [CrossRef]
13. Mertens, J.; Eiden, A.L.; Sigle, D.O.; Huang, F.; Lombardo, A.; Sun, Z.; Sundaram, R.S.; Colli, A.; Tserkezis, C.; Aizpurua, J.; et al. Controlling subnanometer gaps in plasmonic dimers using graphene. *Nano Lett.* **2013**, *13*, 5033–5038. [CrossRef] [PubMed]
14. Lee, K.J.; Kim, S.; Hong, W.; Park, H.; Jang, M.S.; Yu, K.; Choi, S.Y. Observation of Wavelength-Dependent Quantum Plasmon Tunneling with Varying the Thickness of Graphene Spacer. *Sci. Rep.* **2019**, *9*, 1–8. [CrossRef] [PubMed]
15. Losurdo, M.; Yi, C.; Suvorova, A.; Rubanov, S.; Kim, T.H.; Giangregorio, M.M.; Jiao, W.; Bergmair, I.; Bruno, G.; Brown, A.S. Demonstrating the capability of the high-performance plasmonic gallium-graphene couple. *ACS Nano* **2014**, *8*, 3031–3041. [CrossRef] [PubMed]
16. Losurdo, M.; Giangregorio, M.M.; Capezzuto, P.; Bruno, G. Graphene CVD growth on copper and nickel: Role of hydrogen in kinetics and structure. *Phys. Chem. Chem. Phys.* **2011**, *13*, 20836–20843. [CrossRef]
17. Ferrari, A.C.; Meyer, J.C.; Scardaci, V.; Casiraghi, C.; Lazzeri, M.; Mauri, F.; Piscanec, S.; Jiang, D.; Novoselov, K.S.; Roth, S.; et al. Raman spectrum of graphene and graphene layers. *Phys. Rev. Lett.* **2006**, *97*, 1–4. [CrossRef]
18. Palik, E.D. *Handbook of Optical Constants of Solids*; Academic Press: Beaconvale, Parow, 1998.
19. Hanson, G.W. Dyadic Green's functions and guided surface waves for a surface conductivity model of graphene. *J. Appl. Phys.* **2008**, *103*. [CrossRef]
20. Das, A.; Pisana, S.; Chakraborty, B.; Piscanec, S.; Saha, S.K.; Waghmare, U.V.; Novoselov, K.S.; Krishnamurthy, H.R.; Geim, A.K.; Ferrari, A.C.; et al. Monitoring dopants by Raman scattering in an electrochemically top-gated graphene transistor. *Nat. Nanotechnol.* **2008**, *3*, 210–215. [CrossRef]
21. Von Briggs, H.D. Handbook of X-ray and ultraviolet photoelectron spectroscopy. *Phys. Unserer Z.* **1979**, *10*, 30.
22. Davoodi, J.; Safaralizade, M.; Yarifard, M. Molecular dynamics simulation of a Gold nanodroplet in contact with graphene. *Mater. Lett.* **2016**, *178*, 205–207. [CrossRef]
23. Homa, M.; Sobczak, N.; Sobczak, J.J.; Kudyba, A.; Bruzda, G.; Nowak, R.; Giuranno, D.; Pietrzak, K.; Chmielewski, M. Interaction Between Liquid Silver and Graphene-Coated SiC Substrate. *J. Mater. Eng. Perform.* **2018**, *27*, 4140–4149. [CrossRef]
24. Homa, M.; Sobczak, N.; Sobczak, J.J.; Kudyba, A.; Bruzda, G.; Nowak, R.; Pietrzak, K.; Chmielewski, M.; Strupiński, W. Interaction Between Graphene-Coated SiC Single Crystal and Liquid Copper. *J. Mater. Eng. Perform.* **2018**, *27*, 2317–2329. [CrossRef]
25. Albella, P.; Garcia-Cueto, B.; González, F.; Moreno, F.; Wu, P.C.; Kim, T.H.; Brown, A.; Yang, Y.; Everitt, H.O.; Videen, G. Shape matters: Plasmonic nanoparticle shape enhances interaction with dielectric substrate. *Nano Lett.* **2011**, *11*, 3531–3537. [CrossRef] [PubMed]
26. Gutiérrez, Y.; Losurdo, M.; García-Fernández, P.; Sainz de la Maza, M.; González, F.; Brown, A.S.; Everitt, H.O.; Junquera, J.; Moreno, F. Gallium Polymorphs: Phase-Dependent Plasmonics. *Adv. Opt. Mater.* **2019**, *7*, 1900307. [CrossRef]